



Phase-modulated nonreciprocal photon blockade and transmission via optomechanically induced Kerr nonlinearity

Ning Yuan, Shi-Yan Li, Nan Wang, Ting-Ting Dong, and Ai-Dong Zhu ^{*}
Department of Physics, College of Science, Yunnan University, Yunnan, Jilin 133002, China

 (Received 28 January 2024; revised 9 April 2024; accepted 7 May 2024; published 21 May 2024)

We propose a scheme for implementing nonreciprocal transmission and a nonreciprocal photon blockade (PB) in a whispering-gallery-mode optomechanical resonator. By decoupling the mechanical degree of freedom under the Born-Oppenheimer approximation, the system is reduced to one incorporating Kerr-type nonlinearities induced by optomechanical coupling, including self-Kerr nonlinearities of the clockwise (CW) and counterclockwise (CCW) modes and cross-Kerr nonlinearity between these two modes, thereby strong nonreciprocal PB and transmission can be implemented. We demonstrate that the nonreciprocal PB and transmission are sensitive to the relative phase θ between CW and CCW modes, allowing for switching between reciprocity and nonreciprocity of PB and transmission through engineering the relative phase of external driving lasers. Numerical results obtained with experimental parameters validate the feasibility of achieving perfect nonreciprocal PB and transmission. Our paper presents a viable mechanism for the implementation of perfect nonreciprocal PB and transmission, along with a versatile approach of phase modulation, which holds great promise in serving as a chiral single-photon source in unidirectional quantum communications based on quantum nonreciprocal devices.

DOI: [10.1103/PhysRevA.109.053526](https://doi.org/10.1103/PhysRevA.109.053526)

I. INTRODUCTION

Single-photon sources play an important role in quantum communication [1], quantum cryptography [2], and quantum information processing [3]. One approach to achieve a single-photon source is through the implementation of the photon blockade (PB) effect, wherein the excitation of the first photon blocks the excitation of subsequent photons, resulting in the antibunching distribution of photons. Conventional PB is based on the anharmonicity of energy levels, which often requires strong Kerr nonlinearity in the system. In 2010, Liew *et al.* reported a new mechanism called unconventional PB and demonstrated that strong photon antibunching can be achieved in two coupled cavities with weak Kerr nonlinearity [4]. The generated strong antibunching photons are originated from the destructive quantum interference between different transition pathways. Since then, abundant works on unconventional PB have been studied in various systems, including those with second- and third-order nonlinearities [5–8], nonlinear photonic molecules [9,10], quantum plexcitonic systems [11], optomechanical systems [12–14], and a bimodal optical cavity system [15,16].

Cavity optomechanics [17,18], based on radiation pressure mediated light-matter coupling, has become a promising research subject in quantum optics due to its important quantum applications, such as precision sensing and measurement [19–21], optomechanical cooling [22–24], and quantum information processing [25,26]. Compared with other systems, the primary focus of optomechanics lies in quantum effects induced by nonlinear optomechanical coupling. However,

achieving a strong optomechanical interaction modulated by radiation pressure poses a challenge in experiments. Consequently, many efforts have been dedicated to enhancing the nonlinear optomechanical coupling. Heikkilä *et al.* have proposed to enhance the optomechanical coupling between a mechanical and microwave resonator through the charge tuning of the Josephson inductance [27]. Yin *et al.* have demonstrated that the resonant optomechanical interaction can be enhanced through periodic modulation [28]. Zhou *et al.* have reported a scheme for enhancing nonlinearity in an optomechanical system by utilizing atomic coherence [29]. Lemonde *et al.* have experimentally shown the exponential enhancement of the optomechanical coupling strength using only additional linear resources [30]. The whispering-gallery-mode (WGM) resonators have gained much attention in cavity optomechanics due to the advantageous properties of high-quality factors and a small optical mode volume. Some substantial advancements have been made in exploring the statistical properties of photons in WGM resonators [31–36]. Qu *et al.* investigated the photon statistical properties in a WGM optomechanical system by driving two cavity modes simultaneously [37]. Xu *et al.* demonstrated the nonreciprocal transmission and nonreciprocal photon blockade of a weak input optical field through the utilization of nonlinearity and synthetic magnetism [38]. Meanwhile, the Sagnac effect induced by a rotating WGM resonator is often employed to engineer nonreciprocal devices, which enables signal transmission in one direction while blocking it in the opposite direction. Several nonreciprocal phenomena related to the Sagnac effect have been deeply explored in spinning resonators, such as a nonreciprocal photon blockade [39–44], nonreciprocal phonon blockade [45], nonreciprocal phonon laser [46,47], nonreciprocal quantum entanglement [48,49],

^{*}adzhu@ybu.edu.cn

and nonreciprocal chaos [50]. These effects are essential for engineering quantum devices, such as optical circulators [51], isolators [52,53], amplifiers [54,55], and invisible sensing [56,57], which play important roles in chiral information processing networks.

Inspired by the above works, we investigate the controllable nonreciprocal photon blockade and transmission in a WGM resonator optomechanical system which consists of two counterpropagating optical modes [clockwise (CW) and counterclockwise (CCW) modes] and a mechanical mode. Distinguished from previous studies on nonreciprocity based on the Sagnac effect, here we demonstrate that the optomechanically induced Kerr-type nonlinearity and the phase of the driving field can be exploited to manipulate the nonreciprocity of the system. Specifically, by employing the Born-Oppenheimer (BO) approximation [58], the mechanical mode is adiabatically decoupled from two optical modes, resulting in the self-Kerr nonlinearity in both CW and CCW modes, as well as the cross-Kerr nonlinearity between these two modes through the radiation pressure. On the one hand, we find that the PB effect can be observed simultaneously for both the CW mode and CCW mode in the case of single driving. On the other hand, the nonreciprocal transmission and nonreciprocal PB can be realized by tuning the relative phase between the two driving fields in the case of double driving. Additionally, we also investigate the impacts of backscattering-induced coupling and the Kerr-type nonlinearity on photon statistical properties. Our paper presents an alternative regime for manipulating nonreciprocal PB and nonreciprocal transmission, which does not rely on the rotation of the resonator but instead utilizes the phase modulation of the external driving field.

This paper is organized as follows. In Sec. II, we introduce the system and derive the effective Hamiltonian by using the BO approximation. In Sec. III, we present the quantitative measures of the nonreciprocal PB effect and transmission, and demonstrate the validity of the BO approximation by comparing the dynamical evolutions of the second-order correlation function under the original and effective Hamiltonians. Section IV we focus on achieving a perfect nonreciprocal PB by appropriately adjusting the relative phase between two driving fields. In Sec. V, we study the impacts of backscattering and Kerr nonlinearities on the PB effect and demonstrate the high agreement between numerical simulations and analytical results. Additionally, the bidirectional contrast ratio of nonreciprocal PB is also examined. Finally, the conclusions are presented in Sec. VI.

II. SYSTEM AND EFFECTIVE HAMILTONIAN WITH BO APPROXIMATION

As shown in Fig. 1(a), we consider a WGM resonator that supports two counterpropagating optical modes with an identical frequency ω_c , along with a mechanical mode with frequency ω_m . The CW and CCW modes can be excited by injecting two external driving lasers from port 1 and port 2, respectively, and both are coupled to the mechanical mode via radiation pressure. Meanwhile, the presence of surface roughness and material defects in WGM resonators can inevitably cause backscattering losses, resulting in the coupling

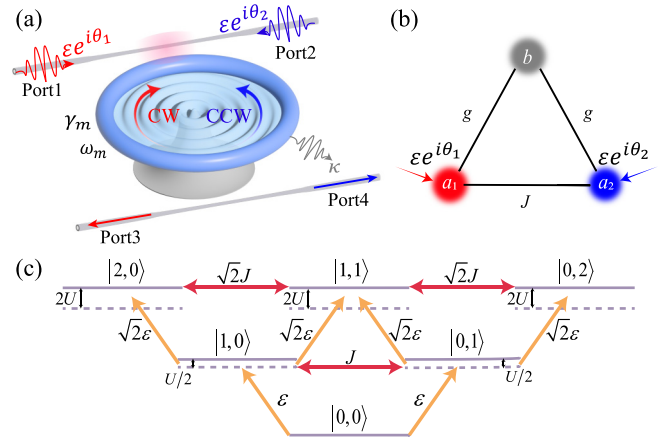


FIG. 1. (a) Schematic of a microdisk WGM resonator with double-driving lasers from opposite directions. The driving fields are evanescently coupled into the CW and CCW modes of the microdisk resonator, where the two degenerate counterpropagating optical modes interact with a mechanical mode through radiation pressure, respectively. (b) A schematic diagram of the intermode couplings of the system. (c) Diagram of the energy-level configuration and the transition paths. The yellow arrows represent the excitations of photons, and the red arrows denote the coherent coupling between the CW and CCW modes.

between the clockwise (CW) and counterclockwise (CCW) modes [59]. Figure 1(b) has illustrated the interactions in the system. In the rotating frame with respect to driving frequency ω_L , the system can be described by the Hamiltonian ($\hbar = 1$)

$$H_1 = \Delta a_{cw}^\dagger a_{cw} + \Delta a_{ccw}^\dagger a_{ccw} + J(a_{cw}^\dagger a_{ccw} + a_{cw} a_{ccw}^\dagger) + \epsilon(a_{cw}^\dagger e^{-i\theta_1} + a_{ccw}^\dagger e^{-i\theta_2} + \text{H.c.}) + H_m, \quad (1)$$

$$H_m = \omega_m b^\dagger b + g(a_{cw}^\dagger a_{cw} + a_{ccw}^\dagger a_{ccw})(b^\dagger + b), \quad (2)$$

where H_m is the Hamiltonian relevant to the mechanical mode including the interaction between the mechanical mode and the coupled optical WGM modes, a (a^\dagger) and b (b^\dagger) stand for the annihilation (creation) operators of optical modes and mechanical mode, respectively, and the subscripts “cw” and “ccw” represent two optical WGM modes. $\Delta = \omega_c - \omega_L$ is the detuning of optical modes, J the strength of the backscattering-induced coupling between the CW and CCW modes, and g the optomechanical coupling strength. θ_j ($j = 1, 2$) and $\epsilon = \sqrt{2\kappa P_{in}/\hbar\omega_L}$ are the phase and amplitude of the driving fields, with P_{in} being the input laser power and κ being the optical decay rate. Noting that the cavity detuning Δ can be tuned by controlling the frequency ω_L of the external driving field so that it can be much smaller than the mechanical frequency ω_m . Under this condition, the mechanical mode can be regarded as a fast variable, allowing for the application of BO approximation to H_m [58].

By introducing the mechanical position and momentum operators with effective mass m , $x = \sqrt{\frac{1}{2m\omega_m}}(b + b^\dagger)$, and $p =$

$-i\sqrt{\frac{m\omega_m}{2}}(b - b^\dagger)$, H_m can be rewritten as

$$\begin{aligned} H_m &= \frac{p^2}{2m} + \frac{1}{2}m\omega_m^2 x^2 + \sqrt{2m\omega_m}g(a_{\text{cw}}^\dagger a_{\text{cw}} + a_{\text{ccw}}^\dagger a_{\text{ccw}})x \\ &= \frac{p^2}{2m} + \frac{1}{2}m\omega_m^2 X^2 - \frac{g^2}{\omega_m}(a_{\text{cw}}^\dagger a_{\text{cw}} + a_{\text{ccw}}^\dagger a_{\text{ccw}})^2, \end{aligned} \quad (3)$$

where $X = x + \sqrt{\frac{2}{m\omega_m^3}}g(a_{\text{cw}}^\dagger a_{\text{cw}} + a_{\text{ccw}}^\dagger a_{\text{ccw}})$ is the mechanical displacement operator which includes a correction induced by the radiation pressure. Then by defining the annihilation operator $A = \sqrt{\frac{m\omega_m}{2}}(X + \frac{ip}{m\omega_m})$, Eq. (3) can be further written as

$$\begin{aligned} H_m &= \omega_m A^\dagger A - U_1 a_{\text{cw}}^\dagger a_{\text{cw}} a_{\text{cw}}^\dagger a_{\text{cw}} - U_2 a_{\text{ccw}}^\dagger a_{\text{ccw}} a_{\text{ccw}}^\dagger a_{\text{ccw}} \\ &\quad - U a_{\text{cw}}^\dagger a_{\text{cw}} a_{\text{ccw}}^\dagger a_{\text{ccw}}, \end{aligned} \quad (4)$$

where $U_1 = U_2 = \frac{g^2}{\omega_m}$ and $U = \frac{2g^2}{\omega_m}$ are the self- and cross-Kerr nonlinearities induced by optomechanical coupling, respectively. It can be seen that under the BO approximation condition, the mechanical mode has been decoupled from these two WGM modes, and strong Kerr nonlinearities can be achieved by varying optomechanical coupling. After performing a unitary transformation $V = \exp[-i\theta_1 a_{\text{cw}}^\dagger a_{\text{cw}} - i\theta_2 a_{\text{ccw}}^\dagger a_{\text{ccw}}]$, the effective Hamiltonian of the system can be written as

$$\begin{aligned} H_{\text{eff}} &= \Delta a_{\text{cw}}^\dagger a_{\text{cw}} + \Delta a_{\text{ccw}}^\dagger a_{\text{ccw}} \\ &\quad + J(a_{\text{cw}}^\dagger a_{\text{ccw}} e^{i\theta} + a_{\text{cw}} a_{\text{ccw}}^\dagger e^{-i\theta}) \\ &\quad - U_1 a_{\text{cw}}^\dagger a_{\text{cw}} a_{\text{cw}}^\dagger a_{\text{cw}} - U_2 a_{\text{ccw}}^\dagger a_{\text{ccw}} a_{\text{ccw}}^\dagger a_{\text{ccw}} \\ &\quad - U a_{\text{cw}}^\dagger a_{\text{cw}} a_{\text{ccw}}^\dagger a_{\text{ccw}} \\ &\quad + \varepsilon(a_{\text{cw}}^\dagger + a_{\text{ccw}}^\dagger + \text{H.c.}), \end{aligned} \quad (5)$$

where $\theta = \theta_1 - \theta_2$ is the phase difference of the two driving lasers. We can see from the above effective Hamiltonian that the parts relevant to the optomechanical interaction in the system are transformed into self-Kerr and cross-Kerr nonlinearities by employing the BO approximation to adiabatically eliminate the mechanical mode. Moreover, the phase difference between the driving fields is also a controllable parameter for implementing the nonreciprocal PB effect and nonreciprocal transmission.

III. SECOND-ORDER CORRELATION FUNCTION AND TRANSMISSION COEFFICIENT

According to the input-output relations [60], we have $a_{1(2),\text{in}} = \varepsilon/\sqrt{\kappa/2}$ and $a_{3(4),\text{out}} = \sqrt{\kappa/2}a_{\text{cw(ccw)}}$ for photons input from port 1(2) and output from port 3(4), then the transmission coefficient can be defined by

$$\begin{aligned} T_{1(2)\rightarrow 3(4)} &\equiv \frac{\langle a_{3(4),\text{out}}^\dagger a_{3(4),\text{out}} \rangle}{\langle a_{1(2),\text{in}}^\dagger a_{1(2),\text{in}} \rangle} \\ &= \frac{\kappa^2}{4\varepsilon^2} \langle a_{\text{cw(ccw)}}^\dagger a_{\text{cw(ccw)}} \rangle. \end{aligned} \quad (6)$$

In addition, the quantum statistical properties of the transmitted photons can be described by equal-time second-order correlation functions in the steady state, i.e., for photons

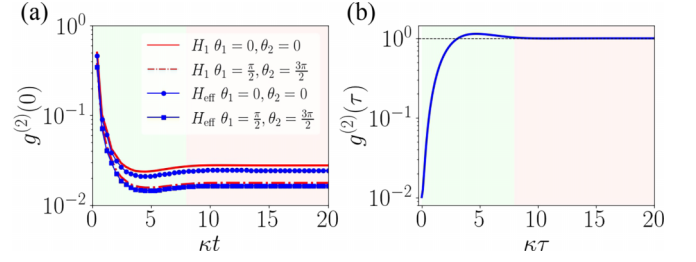


FIG. 2. (a) The dynamical evolution of equal-time second-order correlation functions $g^{(2)}(0)$. The red solid line and red dashed-dotted line represent the correlation function governed by the initial Hamiltonian H_1 in two different cases: $\theta_1 = \theta_2 = 0$ and $\theta_1 \neq \theta_2$, respectively. On the other hand, the blue lines with dots and square markers depict the correlation function governed by the effective Hamiltonian H_{eff} in the above two scenarios. (b) The dynamical evolution of time-delayed second-order correlation function $g^{(2)}(\tau)$ in CW mode (CCW mode) when $\theta_1 = \theta_2 = 0$. The parameters are taken as $J/\kappa = 0.5$, $U/\kappa = 10$, $\Delta/\kappa = 5$, $\omega_m/\kappa = 50$, $\varepsilon/\kappa = 0.01$, $\gamma/\kappa = 0.01$.

transmitted from port 1(2) to port 3(4)

$$\begin{aligned} g_{1(2)\rightarrow 3(4)}^{(2)}(0) &\equiv \frac{\langle a_{3(4),\text{out}}^\dagger a_{3(4),\text{out}}^\dagger a_{3(4),\text{out}} a_{3(4),\text{out}} \rangle}{\langle a_{3(4),\text{out}}^\dagger a_{3(4),\text{out}} \rangle^2} \\ &= \frac{\langle a_{\text{cw(ccw)}}^\dagger a_{\text{cw(ccw)}}^\dagger a_{\text{cw(ccw)}} a_{\text{cw(ccw)}} \rangle}{\langle a_{\text{cw(ccw)}}^\dagger a_{\text{cw(ccw)}} \rangle^2}. \end{aligned} \quad (7)$$

The case of $g^{(2)}(0) < 1$ corresponds to sub-Poisson statistics, implying the photon antibunching effect. Conversely, the case of $g^{(2)}(0) > 1$ corresponds to super-Poisson statistics, referred to as the photon bunching effect. In the limit $g^{(2)}(0) \rightarrow 0$, a complete photon blockade can be observed.

The dynamical evolution of the equal-time second-order correlation function can be obtained by numerically solving the master equation

$$\dot{\rho} = -i[H, \rho] + \frac{\kappa}{2} \mathcal{L}[o]\rho, \quad (8)$$

where $\mathcal{L}[o]\rho = 2o\rho o^\dagger - (o^\dagger o \rho + \rho o^\dagger o)$ ($o = a_{\text{cw}}, a_{\text{ccw}}$) denotes a Lindblad term for operator o .

Here, we take the experimental parameters reported in the Refs. [61,62] to satisfy the condition of BO approximation, i.e., $m = 10$ ng, $\lambda = 1550$ nm, $Q = 10^4 - 10^8$, and $R = 20$ μm . In Fig. 2(a), the dynamical evolution of the equal-time second-order correlation function is depicted governed by the initial Hamiltonian H_1 and the effective Hamiltonian H_{eff} , respectively. It can be observed that the correlation function gradually converges to a stable value less than 1 over time, indicating the sub-Poisson statistics of photons. Furthermore, the second-order correlation function governed by H_{eff} exhibits excellent agreement with that obtained from the initial Hamiltonian H_1 , irrespective of whether θ_1 and θ_2 are equal. This validates the rationality of the effective Hamiltonian under the Born-Oppenheimer approximation when all parameters are satisfied. Meanwhile, the time-delayed second-order correlation function $g^{(2)}(\tau) = \langle a^\dagger(t) a^\dagger(t + \tau) a(t + \tau) a(t) \rangle / \langle a^\dagger(0) a(0) \rangle^2$ is depicted in Fig. 2(b), indicating the conditional probability

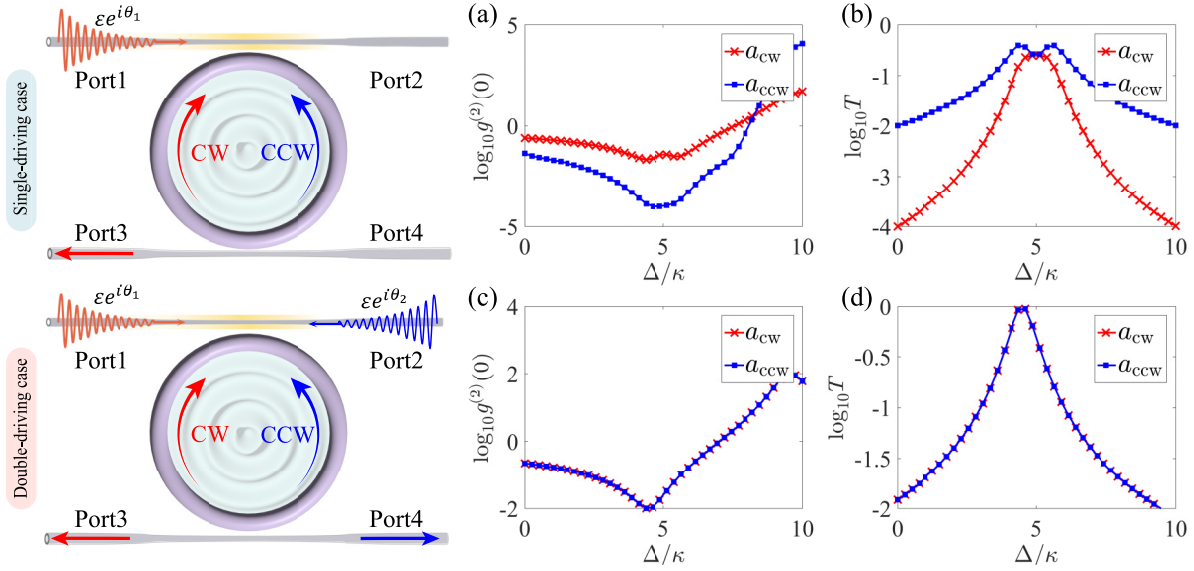


FIG. 3. Exploring the photon statistical properties in the CW mode and CCW mode for single- and double-driving cases. (a) and (b) describe the logarithmic second-order correlation function $g^{(2)}(0)$ and transmission coefficient T vs the detuning Δ/κ under single driving. (c) and (d) illustrate the same analysis for the double-driving case. The parameters are the same as in Fig. 2.

of detecting a second photon at $t + \tau$ given that a photon has been previously detected at time t . Evidently, the antibunching state is observed when $g^{(2)}(\tau) > g^{(2)}(0)$ and $g^{(2)}(0) \ll 1$, indicating that the delayed second-order correlation function gradually approaches 1 as τ increases. This suggests that the photon number distribution tends towards a coherent state at longer time delays, providing clear evidence of photon antibunching.

IV. PHASE-MODULATED NONRECIPROCAL PB AND TRANSMISSION

In this section, we focus on the implementation of nonreciprocal PB and transmission by applying the driving phase. We first consider the case of single driving, i.e., only the CW mode is driven by an external laser field with a phase $\theta_1 = 0$, as illustrated in the first row of Fig. 3. The second-order correlation function $g^{(2)}(0)$ and transmission coefficient T are plotted as functions of the detuning frequency Δ for both two optical modes in Figs. 3(a) and 3(b). The PB effect can be observed simultaneously in both optical modes, but at the optimal PB point $\Delta/\kappa = 5$ these two modes exhibit reciprocal transmission. Second, in the case of double-driving lasers with the phase shift $\theta = 0$, i.e., the CW and CCW modes are driven simultaneously as shown in the second row of Fig. 3, both the PB effect and transmission coefficient exhibit symmetric in CW and CCW modes as shown in Figs. 3(c) and 3(d) due to the symmetry of structure.

The occurrence of the photon antibunching effect can be explained by destructive quantum interference between different transition pathways. As seen from Fig. 1(c), under the condition of single driving on the CW mode, the interference occurs between the pathway $|1, 0\rangle \xrightarrow{\sqrt{2}J} |2, 0\rangle$ and $|1, 0\rangle \xrightarrow{J} |0, 1\rangle \xrightarrow{\varepsilon} |1, 1\rangle \xrightarrow{\sqrt{2}J} |2, 0\rangle$ for the CW mode and between $|1, 0\rangle \xrightarrow{J} |0, 1\rangle \xrightarrow{\sqrt{2}\varepsilon} |1, 1\rangle \xrightarrow{\sqrt{2}J} |0, 2\rangle$ and $|1, 0\rangle \xrightarrow{\sqrt{2}\varepsilon}$

$|2, 0\rangle \xrightarrow{\sqrt{2}J} |1, 1\rangle \xrightarrow{\sqrt{2}J} |0, 2\rangle$ for the CCW mode, thereby the two-photon state $|2, 0\rangle$ and $|0, 2\rangle$ are suppressed. However, in the case of simultaneous driving on both optical modes, additional transition pathways emerge, e.g., $|1, 0\rangle \xrightarrow{\varepsilon} |1, 1\rangle \xrightarrow{\sqrt{2}J} |2, 0\rangle$, $|0, 1\rangle \xrightarrow{\varepsilon} |1, 1\rangle \xrightarrow{\sqrt{2}J} |2, 0\rangle$, and so on, resulting in the perfect symmetry of these transition pathways for CW and CCW modes. Consequently, the two optical modes exhibit reciprocity of the photon statistical properties for $\theta_1 = \theta_2$.

In order to achieve the quantum nonreciprocity of the photons, we modulate the relative phase of external driving fields to implement nonreciprocal PB and transmission. In Fig. 4, the correlation function $g^{(2)}(0)$ and transmission coefficient T are illustrated as functions of the detuning frequency Δ and the relative phase θ . Around the phase shift $\theta = \pi/2$, pronounced antibunching [$g_{1 \rightarrow 3}^{(2)}(0) < 0.01$] is observed in the transmitted photons from port 1 to port 3 in the CW mode, within the region indicated by the red dashed line in Fig. 4(a), accompanied by high transmission ($T_{1 \rightarrow 3} \approx 1$) within the same region as shown in Fig. 4(d). Conversely, a contrasting behavior is observed around $\theta = 3\pi/2$, depicted by the red slender area in Fig. 4(a) and the blue slender area in Fig. 4(d). Meanwhile, the photons transmitted from port 2 to port 4 in the CCW mode exhibit significant antibunching [$g_{2 \rightarrow 4}^{(2)}(0) < 0.01$] within the region indicated by the blue dashed line around $\theta = 3\pi/2$ in Fig. 4(b), along with high transmission ($T_{2 \rightarrow 4} \approx 1$) within the region indicated by the blue dashed line in Fig. 4(e). Similarly, a vice versa behavior is observed around $\theta = \pi/2$. Noticeably, the nonreciprocal PB and nonreciprocal transmission can be achieved for a different relative phase around $\Delta/\kappa = 5$. The dark red and light blue shadows in Figs. 4(c) and 4(f) visually demonstrate the optimal nonreciprocity for $\theta = \pi/2$ and $3\pi/2$, respectively. Physically, the phenomena of the strong antibunching effect and high transmission are caused by the enhanced population

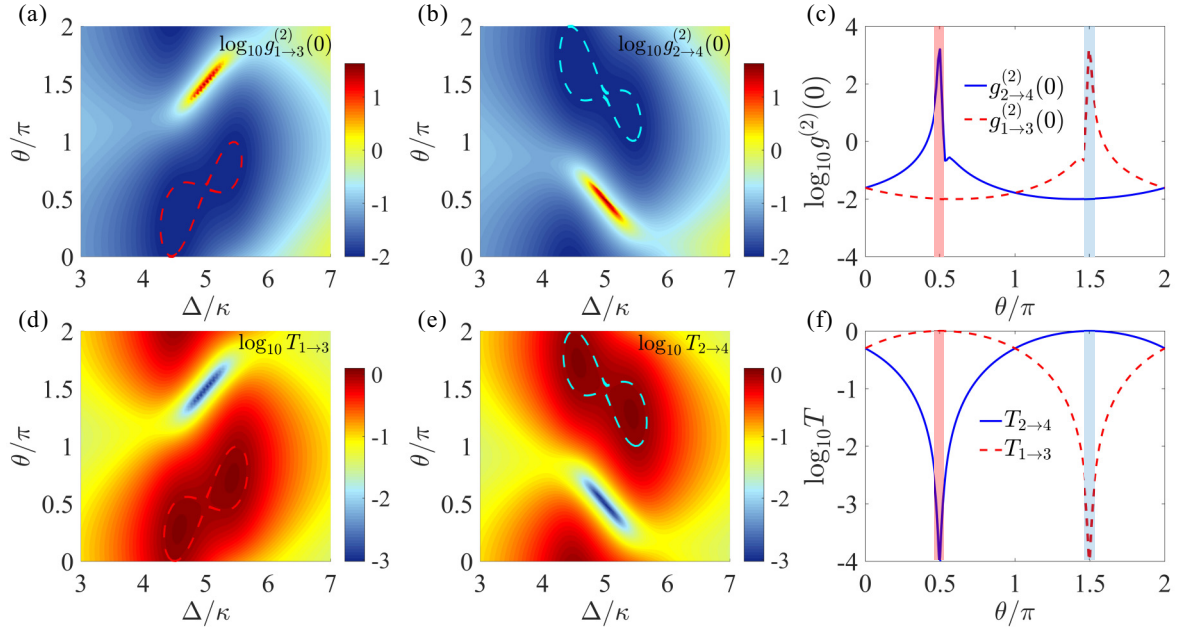


FIG. 4. (a), (b) The logarithmic equal-time second-order correlation function $g_{1(2) \rightarrow 3(4)}^{(2)}(0)$ and (d), (e) transmission coefficient $T_{1(2) \rightarrow 3(4)}$ as a function of the detuning Δ/κ and the relative phase θ/π . (c) $g_{1(2) \rightarrow 3(4)}^{(2)}(0)$ and (f) $T_{1(2) \rightarrow 3(4)}$ vs the phase difference of the double-driving lasers with the detuning $\Delta/\kappa = 5$. The dark red and light blue shades represent the optimal nonreciprocity regions. Other parameters are the same as in Fig. 2.

of single-photon states in the two modes, which originates from the destructive interference between different paths for two-photon excitation.

In general, the physical mechanism of the photon anti-bunching effect can be verified by the equal-time higher-order correlation function

$$g_i^{(n)}(0) = \frac{\langle a_i^\dagger{}^n a_i^n \rangle}{\langle a_i^\dagger a_i \rangle^n} \quad (n > 2). \quad (9)$$

It characterizes the n -PB with the condition of $g_i^{(n)}(0) \geq 1$, $g_i^{(n+1)}(0) < 1$, or photon-induced tunneling with the condition of $g_i^{(n)}(0) > 1$, a phenomenon that the absorption of the first photon contributes to the absorption of subsequent photons. To verify the nonreciprocal single PB, the second-order and third-order correlation functions are depicted versus the detuning Δ/κ for a relative phase $\theta = \pi/2$ in Fig. 5. Figure 5(a)

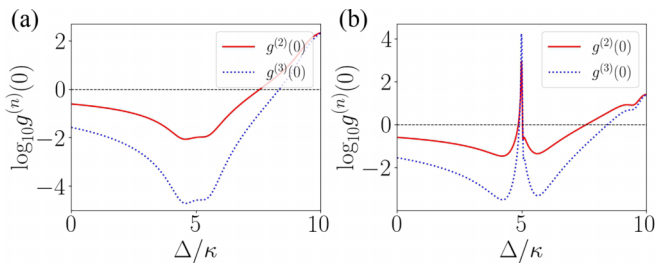


FIG. 5. Logarithmic equal-time second-order correlation function $g_i^{(2)}(0)$ and third-order correlation function $g_i^{(3)}(0)$ vs the detuning Δ/κ for the CW mode in (a) and for the CCW mode in (b) when the relative phase $\theta = \pi/2$. Other parameters are the same as in Fig. 2.

shows the values of $g^{(2)}(0)$ and $g^{(3)}(0)$ less than 1 around the detuning $\Delta/\kappa = 5$ for the CW mode, thereby demonstrates a perfect single PB of the CW mode. Meanwhile, a bunching effect can be observed in the CCW mode as shown in Fig. 5(b), implying photon-induced tunneling for the same condition. In contrast, at a relative phase of $\theta = 3\pi/2$, the CW mode

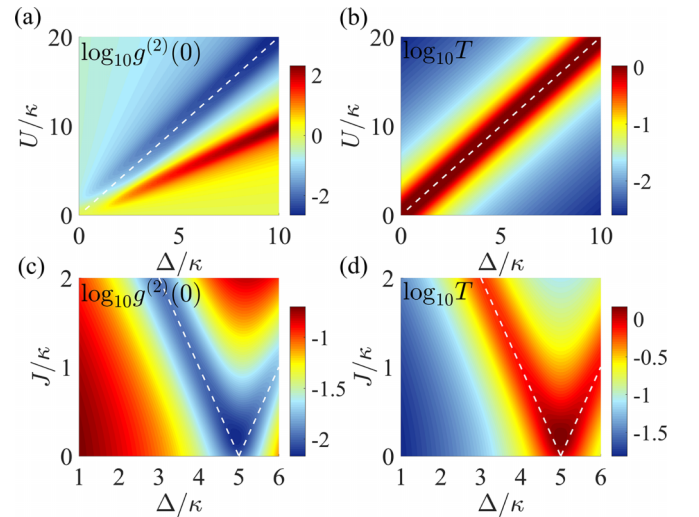


FIG. 6. Logarithmic equal-time second-order correlation function $g^{(2)}(0)$ in (a) and the transmission coefficient T in (b) as functions of Δ/κ and U/κ for $J/\kappa = 0.5$. Logarithmic second-order correlation function $g^{(2)}(0)$ in (c) and the transmission coefficient T in (d) as functions of Δ/κ and J/κ for $U/\kappa = 10$. The white dotted line denotes the analytical solutions in Eq. (11). Other parameters are the same as in Fig. 2.

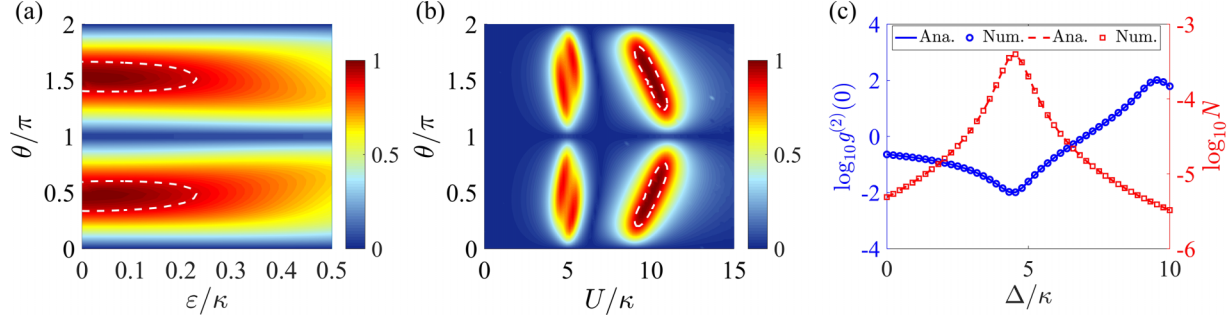


FIG. 7. Influence of driving strength ε/κ in (a) and the Kerr nonlinear strength U/κ in (b) on the bidirectional contrast ratio C , where the white dashed lines denote $C = 0.9$. (c) The equal-time second-order correlation function $g^{(2)}(0)$ and mean photon number N in logarithmic scale vs the optical detuning for the CW (CCW) mode. Numerical results and analytical results are represented by blue circle markers and blue solid lines for the correlation function, respectively. They are also represented by red square markers and red dashed lines for the mean photon number, respectively. Other parameters are the same as in Fig. 2.

exhibits pronounced bunching behavior while the CCW mode demonstrates an antibunching effect, which is not illustrated here. The above features provide a valid method for achieving a unidirectional nonclassical light through external phase modulation, which can be utilized as a quantum unidirectional isolator in quantum networks.

V. ANALYTICAL RESULTS

The quantum statistics of photons can be obtained by solving the Schrödinger equation with a non-Hermitian Hamiltonian that incorporates cavity decay $H_{\text{non}} = H_{\text{eff}} - i\frac{\kappa}{2}a_{\text{cw}}^\dagger a_{\text{cw}} - i\frac{\kappa}{2}a_{\text{ccw}}^\dagger a_{\text{ccw}}$. In the weak driving limit $\varepsilon \ll \kappa$, the occupations for the steady state are obtained as

$$\begin{aligned} C_{10} &= \frac{2\varepsilon(2Je^{i\theta} + A)}{-4J^2 + A^2}, \\ C_{01} &= \frac{2\varepsilon(2Je^{-i\theta} + A)}{-4J^2 + A^2}, \\ C_{20} &= \frac{\varepsilon^2[J^2U + Je^{i\theta}(Je^{i\theta} + 2B)D + 2AB^2]}{\sqrt{2}[(4J^2 - A^2)(J^2 - B^2)B]}, \\ C_{02} &= \frac{\varepsilon^2[J^2U + Je^{-i\theta}(Je^{-i\theta} + 2B)D + 2AB^2]}{\sqrt{2}[(4J^2 - A^2)(J^2 - B^2)B]}, \end{aligned} \quad (10)$$

where C_{nm} denotes the probability amplitude of the state $|n, m\rangle$ with n photons in the CW mode and m photons in the CCW mode and the parameters $\Delta' = \Delta - i\frac{\kappa}{2}$, $A = U - 2\Delta'$,

$B = U - \Delta'$, $D = 3U - 4\Delta'$. Then the analytical expressions of the second-order correlation functions can be calculated as

$$g_{1(2) \rightarrow 3(4)}^{(2)}(0) = \frac{2|C_{20(02)}|^2}{|C_{10(01)}|^4}. \quad (11)$$

From the above expressions, it is clearly that the second-order correlation function $g^{(2)}(0)$ is dependent on the relative phase θ of two external driving fields.

To study the effects of Kerr nonlinearity U and backscattering coupling J on the nonreciprocal PB, the logarithmic second-order correlation function $g^{(2)}(0)$ and transmission coefficient T are plotted versus Δ/κ and U/κ in Figs. 6(a) and 6(b) and versus Δ/κ and J/κ in Figs. 6(c) and 6(d) for the CW mode as the relative phase $\theta = \pi/2$, where the white dashed lines represent the optimal parametric condition obtained from Eq. (11). We noticed that the numerical results exactly coincide with the analytical results, indicating the perfect nonreciprocal PB and transmission can be achieved. Moreover, a stronger nonlinearity strength U is beneficial for enhancing the antibunching effect as shown in Fig. 6(a), while Fig. 6(c) reveals that an overly strong backscattering coupling ($J > \kappa$) between the two modes can weaken the destructive interference between the different transition paths under the current weak driving condition ($\varepsilon < \kappa$), leading to the decline of the photon blockade. For the CCW mode, antibunching and transmission occur as $\theta = 3\pi/2$, which has not been plotted here.

To further quantitatively describe the degree of nonreciprocity, we define a bidirectional contrast ratio C (satisfying $0 \leq C \leq 1$) with the form

$$C = \frac{\left| g_{1 \rightarrow 3}^{(2)}(0) - g_{2 \rightarrow 4}^{(2)}(0) \right|}{\left| g_{1 \rightarrow 3}^{(2)}(0) + g_{2 \rightarrow 4}^{(2)}(0) \right|}, \quad (12)$$

where $C = 1$ corresponds the ideal nonreciprocal PB effect and $C = 0$ implies the reciprocity. From Fig. 7(a) in which the bidirectional contrast ratio C is depicted versus the relative phase θ/π and driving strength ε/κ , we can find weak driving is necessary for achieving a nearly perfect nonreciprocity for the relative phase $\theta = \pi/2$ or $\theta = 3\pi/2$. Meanwhile, the strong nonreciprocity at around $U/\kappa = 5, 10$ can be observed as shown in Fig. 7(b). Moreover, the equal-time second-order correlation function $g^{(2)}(0)$ and mean photon number N ($N =$

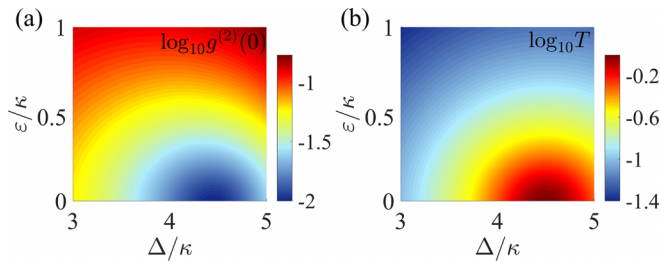


FIG. 8. (a) The logarithmic equal-time second-order correlation function $g^{(2)}(0)$ and (b) transmission coefficient T as a function of the driving strength ε/κ , respectively. Other parameters are the same as in Fig. 2.

$\langle a^\dagger a \rangle$) in the logarithmic scale versus the optical detuning for the CW (CCW) mode are plotted in Fig. 7(c). It can be observed that the peak of the average photon number appears at the detuning with the lowest second-order correlation function. These observations further provide support to the former findings. Finally, the effect of driving strength on nonreciprocity is investigated. As shown in Fig. 8, the second-order correlation function $g^{(2)}(0)$ increases and the transmission coefficient decreases with increasing driving strength ε , which is unfavorable for the PB and transmission. This is attributed to the fact that a strong driving field can introduce additional noise in the resonator, which reduces the probability of the system being in a single-photon state. A weak driving strength also guarantees the optimal nonreciprocity, which is consistent with Fig. 7(a).

VI. CONCLUSIONS

In conclusion, we propose an implementation of nonreciprocal PB and transmission in a WGM optomechanical system. Under the BO approximation, the self- and cross-Kerr nonlinearities are resulted from the optomechanical coupling.

The nonreciprocal PB can be manipulated by adjusting the phase shift θ between external driving fields. Numerical simulations demonstrate that reciprocal unconventional PB can be implemented at $\theta = 0$, while the nonreciprocal PB and transmission can be switched on for the CW mode as the relative phase $\theta = \pi/2$ and for the CCW mode $\theta = 3\pi/2$. Notably, optomechanically induced Kerr nonlinearities play a crucial role in generating antibunching effects, which can be further enhanced by increasing the optomechanical coupling strength. Finally, analysis of the bidirectional contrast ratio C confirms that perfect nonreciprocal PB and transmission are achievable. Our proposed scheme demonstrates an effective regime for quantum nonreciprocity and provides a method of phase manipulation that holds promising potential for applications in chiral single-photon sources, quantum switches, and unidirectional quantum isolators.

ACKNOWLEDGMENTS

This work was supported by the National Natural Science Foundation of China under Grant No. 12264051.

-
- [1] J. Barrett, L. Hardy, and A. Kent, No signaling and quantum key distribution, *Phys. Rev. Lett.* **95**, 010503 (2005).
 - [2] N. Gisin, G. Ribordy, W. Tittel, and H. Zbinden, Quantum cryptography, *Rev. Mod. Phys.* **74**, 145 (2002).
 - [3] W. B. Gao, P. Fallahi, E. Togan, and A. Imamoglu, Observation of entanglement between a quantum dot spin and a single photon, *Nature (London)* **491**, 426 (2012).
 - [4] T. C. H. Liew and V. Savona, Single photons from coupled quantum modes, *Phys. Rev. Lett.* **104**, 183601 (2010).
 - [5] D. Gerace and V. Savona, Unconventional photon blockade in doubly resonant microcavities with second-order nonlinearity, *Phys. Rev. A* **89**, 031803(R) (2014).
 - [6] Y. H. Zhou, H. Z. Shen, and X. X. Yi, Unconventional photon blockade with second-order nonlinearity, *Phys. Rev. A* **92**, 023838 (2015).
 - [7] H. Flayac and V. Savona, Single photons from dissipation in coupled cavities, *Phys. Rev. A* **94**, 013815 (2016).
 - [8] H. Flayac and V. Savona, Input-output theory of the unconventional photon blockade, *Phys. Rev. A* **88**, 033836 (2013).
 - [9] M. Bamba, A. Imamoglu, I. Carusotto, and C. Ciuti, Origin of strong photon antibunching in weakly nonlinear photonic molecules, *Phys. Rev. A* **83**, 021802(R) (2011).
 - [10] X. W. Xu and Y. Li, Strong photon antibunching of symmetric and antisymmetric modes in weakly nonlinear photonic molecules, *Phys. Rev. A* **90**, 033809 (2014).
 - [11] J. B. You, Y. K. Lu, Y. F. Xiao, C. E. Png, F. J. Garcia-Vidal, C. W. Qiu, and L. Wu, Reconfigurable photon sources based on quantum plexcitonic systems, *Nano Lett.* **20**, 4645 (2020).
 - [12] J. Y. Yang, Z. Yang, C. S. Zhao, R. Peng, and L. Zhou, Nonlinearity enhancement and photon blockade in hybrid optomechanical systems, *Opt. Express* **29**, 36167 (2021).
 - [13] B. Sarma and A. K. Sarma, Unconventional photon blockade in three-mode optomechanics, *Phys. Rev. A* **98**, 013826 (2018).
 - [14] X. W. Xu and Y. J. Li, Antibunching photons in a cavity coupled to an optomechanical system, *J. Phys. B: At., Mol. Opt. Phys.* **46**, 035502 (2013).
 - [15] W. Zhang, Z. Y. Yu, Y. M. Liu, and Y. W. Peng, Optimal photon antibunching in a quantum-dot-bimodal-cavity system, *Phys. Rev. A* **89**, 043832 (2014).
 - [16] A. Majumdar, M. Bajcsy, A. Rundquist, and J. V. Vuković, Loss-enabled sub-Poissonian light generation in a bimodal nanocavity, *Phys. Rev. Lett.* **108**, 183601 (2012).
 - [17] M. Aspelmeyer, T. J. Kippenberg, and F. Marquardt, Cavity optomechanics, *Rev. Mod. Phys.* **86**, 1391 (2014).
 - [18] S. Barzanjeh, A. Xuereb, S. Groblacher, M. Paternostro, C. A. Regal, and E. M. Weig, Optomechanics for quantum technologies, *Nat. Phys.* **18**, 15 (2022).
 - [19] T. R. Liu, F. Pagliano, V. Pogorelskiy, Y. Q. Jiao, and A. Fiore, Integrated nano-optomechanical displacement sensor with ultrawide optical bandwidth, *Nat. Commun.* **11**, 2407 (2020).
 - [20] W. Zhao, S. D. Zhang, A. Miranowicz, and H. Jing, Weak force sensing with squeezed optomechanics, *Sci. China: Phys. Mech. Astron.* **63**, 224211 (2020).
 - [21] A. G. Krause, M. Winger, T. D. Blasius, Q. Lin, and O. Painter, A high-resolution microchip optomechanical accelerometer, *Nat. Photonics* **6**, 768 (2012).
 - [22] T. J. Kippenberg and K. J. Vahala, Cavity optomechanics: Backaction at the mesoscale, *Science* **321**, 1172 (2008).
 - [23] J. B. Clark, F. Lecocq, R. W. Simmonds, J. Aumentado, and J. D. Teufel, Sideband cooling beyond the quantum backaction limit with squeezed light, *Nature (London)* **541**, 191 (2017).
 - [24] R. Riedinger, S. K. Hong, R. A. Norte, J. A. Slater, J. Y. Shang, A. G. Krause, V. Anant, M. Aspelmeyer, and S. Gröblacher, Non-classical correlations between single photons and phonons from a mechanical oscillator, *Nature (London)* **530**, 313 (2016).
 - [25] F. Xue, L. Zhong, Y. Li, and C. P. Sun, Analogue of cavity quantum electrodynamics for coupling between spin and

- a nanomechanical resonator: Dynamic squeezing and coherent manipulations, *Phys. Rev. B* **75**, 033407 (2007).
- [26] V. Fiore, Y. Yang, M. C. Kuzyk, R. Barbour, L. Tian, and H. Wang, Storing optical information as a mechanical excitation in a silica optomechanical resonator, *Phys. Rev. Lett.* **107**, 133601 (2011).
- [27] T. T. Heikkilä, F. Massel, J. Tuorila, and M. A. Sillanpää, Enhancing optomechanical coupling via the Josephson effect, *Phys. Rev. Lett.* **112**, 203603 (2014).
- [28] T. S. Yin, L. L. Zheng, M. Zhang, S. Li, and Y. Wu, Nonlinear effects in modulated quantum optomechanics, *Phys. Rev. A* **95**, 053861 (2017).
- [29] L. Zhou, J. Cheng, Y. Han, and W. Zhang, Nonlinearity enhancement in optomechanical systems, *Phys. Rev. A* **88**, 063854 (2013).
- [30] M-A. Lemonde, N. Didier, and A. A. Clerk, Enhanced nonlinear interactions in quantum optomechanics via mechanical amplification, *Nat. Commun.* **7**, 11338 (2016).
- [31] R. Huang, J. Q. Liao, F. Minganti, L. M. Kuang, F. Nori, and H. Jing, Exceptional photon blockade: Engineering photon blockade with chiral exceptional points, *Laser Photonics Rev.* **16**, 2100430 (2022).
- [32] X. F. Liu, T. J. Wang, Y. P. Gao, C. Cao, and C. Wang, Chiral microresonator assisted by Ryberg-atom ensembles, *Phys. Rev. A* **98**, 033824 (2018).
- [33] W. A. Li, Tunable photon blockade in a whispering-gallery-mode microresonator coupled with two nanoparticles, *arXiv:1909.09919*.
- [34] D. Y. Wang, L. L. Yan, S. L. Su, H. F. Wang, and E. J. Liang, Squeezing-induced nonreciprocal photon blockade in an optomechanical microresonator, *Opt. Express* **31**, 22343 (2023).
- [35] J. Y. Sun and H. Z. Shen, Photon blockade in non-Hermitian optomechanical systems with nonreciprocal couplings, *Phys. Rev. A* **107**, 043715 (2023).
- [36] N. Yuan, S. He, S. Y. Li, N. Wang, and A. D. Zhu, Optical noise-resistant nonreciprocal phonon blockade in a spinning optomechanical resonator, *Opt. Express* **31**, 20160 (2023).
- [37] Y. Qu, J. H. Li, and Y. Wu, Interference-modulated photon statistics in whispering-gallery-mode microresonator optomechanics, *Phys. Rev. A* **99**, 043823 (2019).
- [38] X. W. Xu, Y. Li, B. J. Li, H. Jing, and A. X. Chen, Nonreciprocity via nonlinearity and synthetic magnetism, *Phys. Rev. Appl.* **13**, 044070 (2020).
- [39] Y. W. Jing, H. Q. Shi, and X. W. Xu, Nonreciprocal photon blockade and directional amplification in a spinning resonator coupled to a two-level atom, *Phys. Rev. A* **104**, 033707 (2021).
- [40] Y. M. Liu, J. Cheng, H. F. Wang, and X. X. Yi, Simultaneous nonreciprocal conventional photon blockades of two independent optical modes by a two-level system, *Phys. Rev. A* **107**, 063701 (2023).
- [41] C. D. Gou and X. M. Hu, Simultaneous nonreciprocal photon blockade in two coupled spinning resonators via Sagnac-Fizeau shift and parametric amplification, *Phys. Rev. A* **108**, 043723 (2023).
- [42] H. Z. Shen, Q. Wang, J. Wang, and X. X. Yi, Nonreciprocal unconventional photon blockade in a driven dissipative cavity with parametric amplification, *Phys. Rev. A* **101**, 013826 (2020).
- [43] B. J. Li, R. Huang, X. W. Xu, A. Miranowicz, and H. Jing, Nonreciprocal unconventional photon blockade in a spinning optomechanical system, *Photonics Res.* **7**, 630 (2019).
- [44] W. S. Xue, H. Z. Shen, and X. X. Yi, Nonreciprocal conventional photon blockade in driven dissipative atom-cavity, *Opt. Lett.* **45**, 4424 (2020).
- [45] X. Y. Yao, H. Ali, F. L. Li, and P. B. Li, Nonreciprocal phonon blockade in a spinning acoustic ring cavity coupled to a two-level system, *Phys. Rev. Appl.* **17**, 054004 (2022).
- [46] Y. Jiang, S. Maayani, T. Carmon, F. Nori, and H. Jing, Nonreciprocal phonon laser, *Phys. Rev. Appl.* **10**, 064037 (2018).
- [47] Y. Xu, J. Y. Liu, W. J. Liu, and Y. F. Xiao, Nonreciprocal phonon laser in a spinning microwave magnomechanical system, *Phys. Rev. A* **103**, 053501 (2021).
- [48] Z. B. Yang, J. S. Liu, A. D. Zhu, H. Y. Liu, and R. C. Yang, Nonreciprocal transmission and nonreciprocal entanglement in a spinning microwave magnomechanical system, *Ann. Phys.* **532**, 2000196 (2020).
- [49] Y. F. Jiao, J. X. Liu, Y. Li, R. H. Yang, L. M. Kuang, and H. Jing, Nonreciprocal enhancement of remote entanglement between nonidentical mechanical oscillators, *Phys. Rev. Appl.* **18**, 064008 (2022).
- [50] D. W. Zhang, L. L. Zheng, C. You, C. S. Hu, and Y. Wu, Nonreciprocal chaos in a spinning optomechanical resonator, *Phys. Rev. A* **104**, 033522 (2021).
- [51] M. Scheucher, A. Hilico, E. Will, and A. Rauschenbeutel, Quantum optical circulator controlled by a single chirally coupled atom, *Science* **354**, 1577 (2016).
- [52] C. Sayrin, C. Junge, R. Mitsch, B. Albrecht, and A. Rauschenbeutel, Nanophotonic optical isolator controlled by the internal state of cold atoms, *Phys. Rev. X* **5**, 041036 (2015).
- [53] L. Tang, J. Tang, W. Zhang, G. Lu, H. Zhang, and M. Xiao, On-chip chiral single-photon interface: Isolation and unidirectional emission, *Phys. Rev. A* **99**, 043833 (2019).
- [54] D. Malz, N. R. Bernier, A. K. Feofanov, T. J. Kippenberg, and A. Nunnenkamp, Quantum-limited directional amplifiers with optomechanics, *Phys. Rev. Lett.* **120**, 023601 (2018).
- [55] Z. Shen, Y. L. Zhang, Y. Chen, F. W. Sun, X. B. Zou, G. C. Guo, C. L. Zou, and C. H. Dong, Reconfigurable optomechanical circulator and directional amplifier, *Nat. Commun.* **9**, 1797 (2018).
- [56] H. Jing, H. Lü, S. K. Özdemir, T. Carmon, and F. Nori, Nanoparticle sensing with a spinning resonator, *Optica* **5**, 1424 (2018).
- [57] R. Fleury, D. Sounas, and A. Alù, An invisible acoustic sensor based on parity-time symmetry, *Nat. Commun.* **6**, 5905 (2015).
- [58] Z. R. Gong, H. Ian, Y. X. Liu, C. P. Sun, and F. Nori, Effective Hamiltonian approach to the Kerr nonlinearity in an optomechanical system, *Phys. Rev. A* **80**, 065801 (2009).
- [59] T. J. Kippenberg, S. M. Spillane, and K. J. Vahala, Modal coupling in traveling-wave resonators, *Opt. Lett.* **27**, 1669 (2002).
- [60] C. W. Gardiner and M. J. Collett, Input and output in damped quantum systems: Quantum stochastic differential equations and the master equation, *Phys. Rev. A* **31**, 3761 (1985).
- [61] G. C. Righini, Y. Dumeige, P. Féron, M. Ferrari, G. N. Conti, D. Ristic, and S. Soria, Whispering gallery mode microresonators: Fundamentals and applications, *Riv. Nuovo Cimento* **34**, 435 (2011).
- [62] M. Soltani, S. Yegnanarayanan, and A. Adibi, Ultra-high Q planar silicon microdisk resonators for chip-scale silicon photonics, *Opt. Express* **15**, 4694 (2007).